Loss of Bardet–Biedl syndrome protein-8 (BBS8) perturbs olfactory function, protein localization, and axon targeting

Abigail L. D. Tadenev[a], Heather M. Kulaga[a], Helen L. May-Simera[b], Matthew W. Kelley[b], Nicholas Katsanis[c], and Randall R. Reed[a,1]

[a]Center for Sensory Biology, Department of Molecular Biology and Genetics, School of Medicine, The Johns Hopkins University, Baltimore, MD 21205; [b]Laboratory of Cochlear Development, National Institute on Deafness and Other Communication Disorders, National Institutes of Health, Bethesda, MD 20892; and [c]Center for Human Disease Modeling, Departments of Cell Biology and Pediatrics, Duke University, Durham, NC 27710

Edited by King-Wai Yau, The Johns Hopkins School of Medicine, Baltimore, MD, and approved May 10, 2011 (received for review November 5, 2010)

Bardet–Biedl syndrome (BBS) is a pleiotropic, heterogeneous human disease whose etiology lies primarily in dysfunctional basal bodies and/or cilia. Both BBS patients and several BBS mouse models exhibit impaired olfactory function. To explore the nature of olfactory defects in BBS, a genetic ablation of the mouse *Bbs8* gene that incorporates a fluorescent reporter protein was created. The endogenous BBS8 protein and reporter are particularly abundant in olfactory sensory neurons (OSNs), and specific BBS8 antibodies reveal staining in the dendritic knob in a shell-like structure that surrounds the basal bodies. *Bbs8*-null mice have reduced olfactory responses to a number of odorants, and immunohistochemical analyses reveal a near-complete loss of cilia from OSNs and mislocalization of proteins normally enriched in cilia. To visualize altered protein localization in OSNs, we generated a *SLP3*^{eGFP} knock-in mouse and imaged the apical epithelium, including dendritic knobs and proximal cilia, in ex vivo tissue preparations. Additionally, protein reagents that reflect the characteristic neuronal activity of each OSN revealed altered activity in *Bbs8*-null cells. In addition to previously known defects at the ciliary border, we also observed aberrant targeting of OSN axons to the olfactory bulb; axons expressing the same receptor display reduced fasciculation and project to multiple targets in the olfactory bulb. We suggest that loss of BBS8 leads to a dramatic and variable reduction in cilia, the essential signaling platform for olfaction, which alters the uniformity of responses in populations of OSNs expressing the same receptor, thereby contributing to the observed axon-targeting defects.

ciliopathy | olfactory activity | protein trafficking

Bardet–Biedl syndrome (BBS), a heterogeneous human disease, encompasses pleiotropic phenotypes including obesity, polydactyly, retinal degeneration, and renal anomalies. The disease, associated with mutations in at least 16 genes, shows complex inheritance. The *BBS8* gene was identified via shared homology with *BBS4* and was recognized to bear similarity to bacterial pilF; pilF is thought to be involved in the assembly of pili, which are thin, hairlike extensions on prokaryotic cells (1). This prompted the hypothesis that BBS is primarily a disease of the basal body, a microtubule-based modified centriole that nucleates the ciliary axoneme. Subsequent work supports this common etiology of BBS (2). Characterized BBS genes are highly conserved exclusively among ciliated eukaryotes, and most BBS proteins localize to the basal body, centrosome, and/or cilium in ciliated cell-culture models and in ciliated tissues. BBS proteins are not thought to be essential structural proteins as the basal body and cilium remain largely intact in most mutant BBS models (3–5). Disruption of individual BBS genes leads to defects in intraflagellar transport (IFT), a process essential for protein trafficking within the cilium (6–8).

Recent studies have found that seven BBS proteins—BBS1, -2, -4, -5, -7, -8, and -9—assemble into a complex, the BBSome (9). This complex functions in biogenesis of the ciliary membrane (9), trafficking some proteins to or within the ciliary compartment (10), and/or coordinating IFT particle assembly or movement (7, 8). Recently, BBSome complexes were shown to form a coat on membranes in vitro (11); this polymerization might underlie some of the functions of the complex.

In sensory systems, BBS proteins facilitate protein transport into specialized cilia. Rhodopsin mislocalizes within BBS-null photoreceptors, preceding the apoptotic death of these cells (3, 4, 12–14). Reduced olfactory acuity has also been recognized in BBS patients and was variable, but with >50% penetrance (15). The anosmia phenotype was observed in mouse models of BBS (4, 13, 15–17) where it was associated with a dramatic decrease in structural and signal transduction proteins in the ciliary layer of the olfactory epithelium (OE), suggesting a near-complete loss of olfactory cilia (15). Olfactory sensory neurons (OSNs) extend elaborate cilia, among the longest in the body, that house all necessary components for olfactory signal transduction. The physiological and histological changes in BBS are consistent with the pathology of basal bodies and resulting loss of cilia but, importantly, the OSNs are largely retained in this sensory system.

To further examine olfactory phenotypes in BBS, we genetically ablated *Bbs8* in mice. In addition to elucidating mechanisms of protein transport to and within cilia, we have used this model to examine the consequences of alterations in cilia structure on the ability of OSNs to properly project axons to the olfactory bulb (OB). We show that *Bbs8*-null mice are viable and exhibit olfactory deficits. We also created a *SLP3*^{eGFP} knock-in mouse that allows visualization of an OSN-enriched protein in live, whole-mount tissue. *Bbs8*-null mice show defects in axon targeting, and using a surrogate marker for neuronal activity, we demonstrate increased and highly variable OSN activity levels in mutants. We hypothesize that loss of BBS8 causes defects in cilia structure and function that lead to alterations in signaling activity levels, which contribute to the axon-targeting phenotype.

Results

Expression of *Bbs8* in the Olfactory System. We first examined the expression of both *Bbs8* message and BBS8 protein in the olfactory system. As expected from the predominant expression of BBS genes in ciliated cells, *Bbs8* is abundantly expressed in the neuron layer of the OE, where the OSN cell bodies are found (Fig. 1*A*). BBS8 was previously localized to the mucosal surface of the OE (1); we generated antibodies to a C-terminal peptide of BBS8 to more precisely resolve its localization in OSNs (Fig. 1*B*). BBS8 primarily localizes to the dendritic knobs, swellings at the apical

Author contributions: A.L.D.T., M.W.K., N.K., and R.R.R. designed research; A.L.D.T., H.M.K., and H.L.M.-S. performed research; A.L.D.T. and R.R.R. analyzed data; and A.L.D.T. and R.R.R. wrote the paper.

The authors declare no conflict of interest.

This article is a PNAS Direct Submission.

[1]To whom correspondence should be addressed. E-mail: rreed@jhmi.edu.

This article contains supporting information online at www.pnas.org/lookup/suppl/doi:10.1073/pnas.1016531108/-/DCSupplemental.

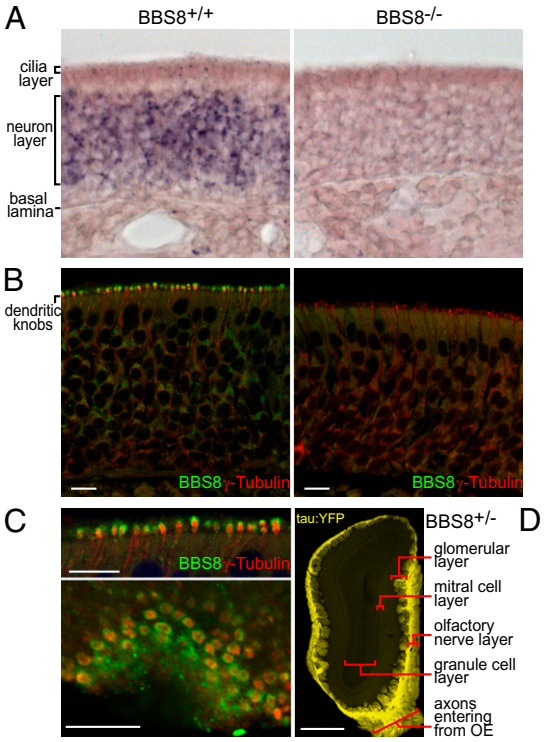

Fig. 1. Genetic ablation of the *Bbs8* gene. (*A*) In situ hybridization reveals *Bbs8* mRNA enrichment in OE neurons (*Left*) and absence in the OE of $Bbs8^{-/-}$ mice (*Right*). (*B*) Immunofluorescence localizes BBS8 protein (green) predominantly to dendritic knobs marked by γ-tubulin (red), a basal body protein. The BBS8 protein signal is absent in $Bbs8^{-/-}$ tissue but γ-tubulin staining persists (*Right*). (*C*) High-magnification image of OE cryosections at the cilia layer reveals distinct localization within the dendritic knob, as seen in a cross-section (*Upper*, a higher magnification of *B*) and in an en face section (*Lower*). The basal body-associated γ-tubulin staining resides in the core of each knob, and the BBS8 immunofluorescence forms a surrounding shell. (*D*) Low-power image of an OB cryosection from a $Bbs8^{+/-}$ mouse reveals intense intrinsic fluorescence from the tau:YFP reporter. Signal is seen specifically in OSN axons projecting from the OE through the olfactory nerve layer and terminating in the olfactory glomeruli. [Scale bar: 10 μm (*B* and *C*); 500 μm (*D*).]

end of OSNs containing the basal bodies of olfactory cilia. Some signal is also observed within the neuron layer, concentrated in the endoplasmic reticulum/Golgi region apical to the nucleus. Notably, within the dendritic knob, confocal microscopy reveals that BBS8 does not overlap with γ-tubulin, a pericentriolar matrix marker. Instead, BBS8 surrounds the γ-tubulin in the dendritic knob, placing it in closer proximity to the connection with the ciliary base (Fig. 1 *B* and *C*). BBS8 is thus located close to the membrane, consistent with the proposed BBSome function as a coat protein (11).

Genetic Ablation of *Bbs8*. Mouse *Bbs8* maps to chromosome 12 and encodes alternatively spliced isoforms (1, 18) that are predicted to generate proteins of ~57 kDa containing multiple tetratricopeptide repeats but few other recognizable domains. To generate a null allele, *Bbs8* was targeted for genetic ablation by elimination of coding sequences in the first two exons (Fig. S1). A tau-YFP cassette and downstream SV40 poly(A) site were inserted at the initiation codon for BBS8. The construct was introduced into mouse ES cells, and homologous integrants were identified by positive-negative selection and Southern blot. This gene disruption strategy replaced 15.8 kb of *Bbs8* genomic sequence and provided a reporter under the control of the *Bbs8* promoter. The in situ hybridization and immunofluorescence signals for *Bbs8* message and protein are below the limit of detection in *Bbs8*-null mice (Fig. 1 *A* and *B*), suggesting successful ablation of the gene and demonstrating antibody specificity.

In crosses of heterozygous mice, $Bbs8^{+/+}$, $Bbs8^{+/-}$, and $Bbs8^{-/-}$ progeny are produced at roughly the expected 1:2:1 frequency. $Bbs8^{-/-}$ animals appear normal at birth, but gain weight slowly and are notably smaller than littermates by PD3. $Bbs8^{-/-}$ mice frequently die before weaning, and homozygous knockout pups are under-represented in litters at PD21 (Fig. S2*A*). However, reduction of litter size and use of supplemental food and water improves survival. By PD70, *Bbs8*-null animals display weights comparable to wild-type (WT) and heterozygous littermates. Like other BBS mice, $Bbs8^{-/-}$ mice become obese, and this effect is more pronounced in female mice (Fig. S2*B*). *Bbs8*-null mice also display retinal degeneration and mislocalization of rhodopsin to photoreceptor inner segments (Fig. S3 *A* and *B*), similar to other BBS mice (3, 13). BBS8 also localized to the connecting cilium region of photoreceptor outer segments in the retina (Fig. S3*C*), agreeing with previous findings (1). Additionally, $Bbs8^{-/-}$ kidneys exhibit mild dilation of the tubules in the deep cortex (Fig. S3*D*). Among nearly 50 mutant mice, no polydactyly and situs inversus were observed; however, these phenotypes occur with low penetrance in human BBS patients. $Bbs8^{+/-}$ animals showed no significant differences from WT and were used interchangeably as experimental controls.

The *Bbs8*-null mouse generated for the present study was specifically engineered with a sufficiently robust reporter under the regulation of endogenous elements to examine the distribution and timing of expression of the target gene. We found that the *Bbs8* promoter-driven tau:YFP reporter is abundant in mature OSNs and, due to the association of the reporter with microtubules, enriches in axon bundles and the nerve and glomerular layers of the OB (Fig. 1*D*). The intense signal in projections of primary OSN axons compared with the intrinsic mitral, periglomerular, and granule cells of the bulb likely reflects the elaborate cilia of the primary sensory neurons. The *Bbs8* locus is also actively transcribed, albeit at lower levels, in a number of other adult tissues, including the retina, kidney, and lung, as shown by both quantitative RT-PCR and Western analyses (Fig. S4).

Loss of BBS8 Reduces Olfactory Sensitivity and Causes Structural and Protein Localization Defects in OE. We next examined the olfactory sensitivity of *Bbs8*-null mice. The proposed etiology of BBS as defects in basal bodies/cilia and the crucial role of olfactory cilia for odorant signal transduction suggested that null mice would have a reduced response to odorants. In electro-olfactogram (EOG) recordings, $Bbs8^{-/-}$ mice exhibited a fivefold reduction in odorant-evoked activity compared with $Bbs8^{+/-}$ littermates (Fig. 2); responses observed for several odorants demonstrated a broad defect in olfactory capability. Thus, *Bbs8*-null mice have a decreased olfactory function, comparable to that seen in *Bbs1* and *Bbs4* mouse models (15).

Sections of mouse olfactory tissue were examined by immunohistochemistry to investigate the molecular basis for the loss of olfactory sensitivity. Acetylated tubulin, which marks stable microtubules (typically enriched in dendrites and cilia), revealed a dramatic reduction in cilia in $Bbs8^{-/-}$ mice (Fig. 3*A*). Cilia loss with cell retention is seen in the olfactory system (15) but not in other ciliated tissues (3–5), perhaps indicating that OSNs are especially sensitive to perturbations in cilia function. The microtubule bundles that label OSN dendrites also appeared disorganized and slightly reduced in number; this could be explained by the modest decrease in OE thickness seen in $Bbs8^{-/-}$ OE. Despite the lack of cilia, basal bodies visualized by γ-tubulin staining were still largely present, although perhaps somewhat reduced in number and intensity (Fig. 1*B*). The OSN-specific transduction protein adenylyl cyclase (ACIII) and stomatin-like protein 3 (SLP3) show greatly reduced signal at the cilia layer in *Bbs8*-null tissue. This is consistent with considerable loss of cilia because these proteins are enriched in WT OSN cilia (Fig. 3 *B* and *C*). ACIII also mislocalized within OSNs, showing more

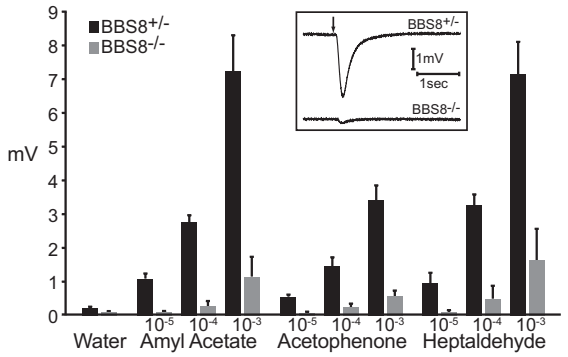

Fig. 2. *Bbs8*$^{-/-}$ mice exhibit reduced responses to odorants. Peak voltage responses in EOG recordings from *Bbs8*$^{+/-}$ or *Bbs8*$^{-/-}$ OE exposed to odorants at the indicated molar concentrations. Each bar represents the average responses for *Bbs8*$^{+/-}$ (n = 12 electrodes/4 mice) or *Bbs8*$^{-/-}$ mice (n = 13 electrodes/4 mice) ± SD. (*Inset*) Representative responses to a pulse of 10^{-4} M amyl acetate.

intense labeling in the dendrite and cell body in *Bbs8*$^{-/-}$ compared with *Bbs8*$^{+/-}$ mice; in addition, SLP3 expression was heterogeneous, with cells exhibiting variable staining intensity. SLP3 mislocalization has also been observed in dorsal root ganglion neurons of other BBS models (19). We next assessed the distribution of olfactory receptor (OR) protein in individual OSNs using an antibody against ORI7, expressed by ~0.1% of OSNs. The ORI7-labeled cells clearly revealed the morphology of individual OSN dendrites and the elaboration of cilia. Consistent with the results of acetylated tubulin staining, single cells in *Bbs8*-null OE have only short cilia and an abnormal accumulation of ORI7 protein within the apical dendrite (Fig. 3 *B* and *C*).

As a complementary approach to directly examining the extent of cilia loss in *Bbs8*$^{-/-}$ OE, we visualized the mucosal surface by scanning electron microscopy (SEM) (Fig. 3*D*). Consistent with our immunofluorescence data, WT mice display a thick layer of densely packed cilia. In mutant mice, the dense cilia are replaced by scattered cilia apparent above a surface of sustentacular cell microvilli.

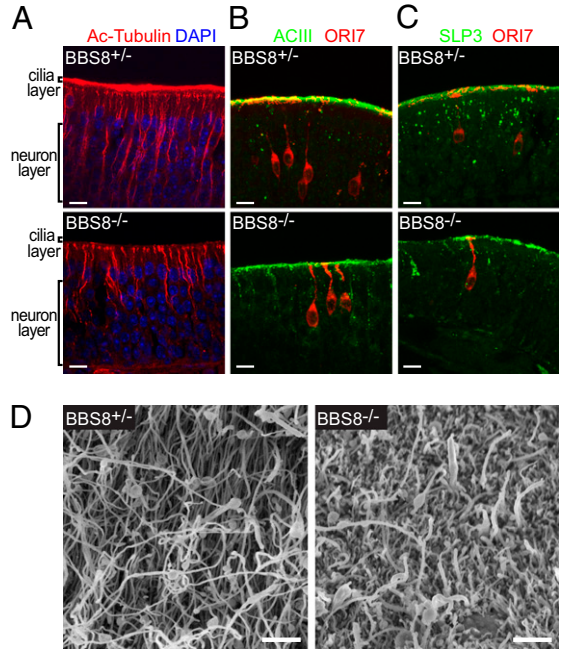

Fig. 3. Structural and protein localization defects in *Bbs8*$^{-/-}$ OE. OE cryosections from *Bbs8*$^{+/-}$ or *Bbs8*$^{-/-}$ animals were immunostained and imaged by confocal microscopy (*A*: single plane, *B* and *C*: flattened Z-stacks). (*A*) Cilia abundance, visualized by acetylated tubulin, is dramatically reduced in *Bbs8*$^{-/-}$ mice. (*B*) The signal transduction proteins ACIII and ORI7 show reduced intensity in the cilia layer and mislocalization within the dendrite in *Bbs8*$^{-/-}$ OE. (*C*) SLP3 shows reduced signal at the cilia layer and accumulation within the dendrite and apical cell body. (*D*) SEM of the olfactory epithelium of 37-wk-old littermates. [Scale bar: 10 μm (*A*–*C*); 2 μm (*D*).]

Protein Mislocalization Is Observed in Vivo. To further explore the observed protein mislocalization in the dendritic knob and cilia of OSNs, we generated a fusion of enhanced green fluorescent protein (eGFP) to SLP3, a stomatin-like protein that is abundant in OSNs and enriched in the dendrite and dendritic knob (20). Knock-in of eGFP to the *SLP3* endogenous locus (Fig. S5*A*) allows for the visualization of the fusion protein, which should be expressed at normal levels in unfixed tissue.

We first assessed whether the localization of the SLP3:eGFP fusion protein accurately mimics that of the endogenous protein in the *Bbs8*$^{+/+}$ background. Analysis of fixed OE sections from WT and *SLP3*$^{+/eGFP}$ animals for SLP3 and SLP3:eGFP by immunohistochemistry and intrinsic fluorescence, respectively, reveals largely similar patterns (Fig. S5*B*). Both SLP3 and SLP3:eGFP localize to puncta within the dendrite layer of OSNs, with diffuse signal at the cilia layer.

We next established a method for imaging the cilia layer en face by confocal microscopy in unfixed tissue and defined SLP3:eGFP localization within individual OSNs. This preparation allows high-resolution imaging of intact cilia and avoids artifacts associated with tissue fixation and sectioning. In the cilia layer of control mice, the SLP3:eGFP fusion protein localizes to the membrane of the dendritic knob and proximal portions of olfactory cilia, resulting in a starburst pattern that repeats across the surface of the OE (Fig. 4) and can be seen clearly at higher magnification (Fig. 4, *Right*). We then examined the distribution of the fusion protein in *Bbs8*$^{+/-}$ and *Bbs8*$^{-/-}$ animals (Fig. 5). The contribution of the *Bbs8*-driven tau:YFP reporter to the fluorescent signal was modest but was eliminated by linear unmixing of the two fluorochromes. Each panel in Fig. 5 represents a single confocal plane, and as the tissue is not perfectly flat, knobs are not seen across the entire field. Rather, the SLP3:eGFP-rich knobs and proximal cilia are superficial to the tau:YFP-rich dendrites. The starburst pattern was highly stereotyped across OSNs in different regions of the OE and across different animals. In contrast, SLP3:eGFP in *Bbs8*-null OSNs shows mosaicism in its expression level among different OSNs and is not restricted to the proximal region of cilia (Fig. 5). Instead, the fusion protein extends throughout the length of some cilia, revealing swellings along the length of the axoneme as has been observed in other BBS models (4, 21). The tau:YFP signal is more intense in the *Bbs8*-null because these animals carry two

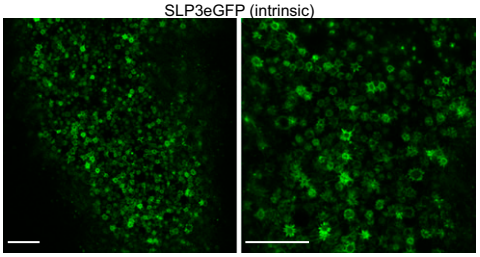

Fig. 4. Localization of endogenous SLP3 in OSNs. SLP3:eGFP localizes to the dendritic knob and proximal regions of cilia in low-power (*Left*) and high-power (*Right*) confocal images of the apical surface of unfixed whole-mount OE at the level of the dendritic knobs. The membrane that forms the surface of the dendritic knob and the proximal portions of cilia appear as a "starburst" pattern when visualizing the intrinsic SLP3:eGFP signal. (Scale bar: 20 μm.)

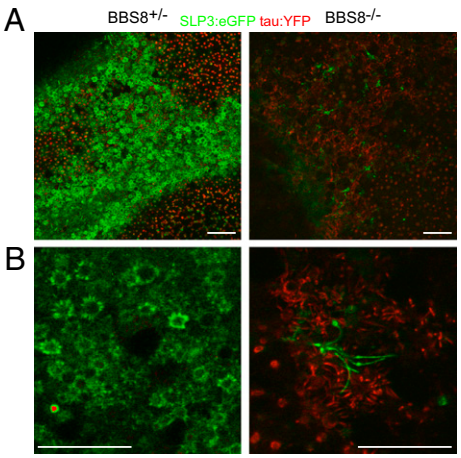

Fig. 5. SLP3:eGFP expression and localization is altered in *Bbs8*$^{-/-}$ OSNs. The fluorescent signals from the *Bbs8* promoter-driven tau:YFP reporter (red) and SLP3:eGFP (green) were separated by linear unmixing. (*A*) In en face images of the cilia layer, SLP3:eGFP is expressed in most, if not all, dendritic knobs of *Bbs8*$^{+/-}$ mice, but is visible in only a few scattered cells of the *Bbs8*$^{-/-}$ OE. (*B*) At high magnification, the altered localization of SLP–3eGFP in *Bbs8*$^{-/-}$ OSNs is apparent. Specifically, in *Bbs8*$^{+/-}$ OE, SLP3:eGFP is restricted to the dendritic knob and proximal cilia (*A* and *B*, *Left*). In *Bbs8*$^{-/-}$ OE (*A* and *B*, *Right*), it is distributed along the length of longer ciliary processes, which also display unusual swellings throughout the extent of the cilia. (Scale bar: 20 μm.)

alleles of the linked reporter. We were intrigued to see SLP3:eGFP localize to long cilia in *Bbs8*$^{-/-}$ tissue, given the near-complete loss of cilia suggested by acetylated tubulin staining and SEM. However, our data suggest that these cilia are rare, consistent with the residual signal that remains in the cilia layer for acetylated tubulin, ACIII, ORI7, and SLP3 (Fig. 3).

Loss of BBS8 Alters Activity Profiles of OSNs. The observed defects in cilia and transduction component distribution suggest that *Bbs8*-null OSNs may exhibit a perturbed location of transduction or spontaneous signaling activity. Previous studies indicated a role for OR levels and associated transduction activity in appropriate axon targeting to the OB by regulation of axon guidance molecule levels (22, 23). Bicistronic transcription of the M72 OR mRNA with the tau:lacZ reporter (M72^{TL}) allows for visualization of soma and axonal projections for OSNs expressing the same OR. To quantify activity levels in individual OSNs expressing a specific OR, we immunostained sections from *Bbs8*$^{+/-}$/M72$^{+/TL}$ and *Bbs8*$^{-/-}$/M72$^{+/TL}$ mice with an antibody against S100A5, a Ca^{2+}-binding protein whose message and protein abundance is correlated with activity in OSNs (Fig. 6) (24). We determined the mean fluorescence signal intensity for both S100A5 and lacZ within the cell body, and S100A5 levels were normalized to lacZ levels to account for differences in antibody accessibility. Normalized S100A5 mean pixel intensity was determined for 10 cells from each of 6 animals (totaling 30 *Bbs8*$^{+/-}$ and 30 *Bbs8*$^{-/-}$ OSNs) (Fig. 6). The abundance of S100A5 differed between the genotypes in two respects. First, the mean intensity was greater, suggesting higher activity in *Bbs8*-null M72 cells (mean = 52.1 for *Bbs8*$^{-/-}$, mean = 28.7 for *Bbs8*$^{+/-}$; $P < 0.001$). Second, the variance in mean S100A5 intensity was much greater for *Bbs8*$^{-/-}$ compared with control (554.76 vs. 54.35, $P < 0.001$). A similar experiment was performed for ORI7-expressing OSNs with similar results (Fig. S6).

Disruption of *Bbs8* Causes Defects in OSN Axon Targeting. Several studies have examined the fidelity of OSN axon targeting under conditions where expression of olfactory signal transduction components and related proteins has been altered by gene ablation (25, 26). However, analogous experiments have not been undertaken when cilia structure or function has been directly

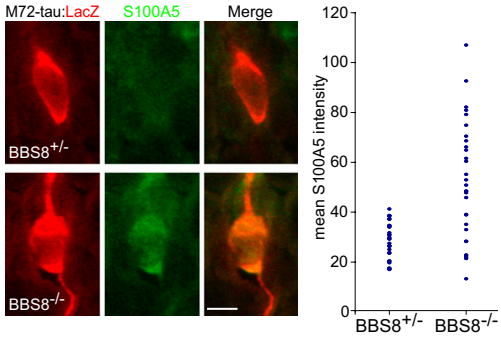

Fig. 6. *Bbs8*$^{-/-}$ OSNs display increased variability in S100A5 protein expression. Sections of OE from *Bbs8*/M72^{TL} mice were stained for lacZ and S100A5 to determine the expression level of S100A5 in individual OSNs from a defined OR population. Images show a lacZ-positive *Bbs8*$^{+/-}$ OSN with relatively low S100A5 levels (*Upper* panels) and a *Bbs8*$^{-/-}$ OSN with high S100A5 levels (*Lower* panels). (*Graph*) The mean S100A5 pixel fluorescence intensity, normalized to lacZ intensity, was determined within each cell body for 30 M72-expressing OSNs ($n = 3$ animals) for each genotype. (Scale bar: 5 μm.)

affected while retaining intact transduction machinery genes. Therefore, we performed whole-mount histochemistry to examine axon targeting in *Bbs8*-null mice carrying the M72^{TL} allele (25). In dorsal-view preparations from WT mice, lacZ-positive axons course over the dorsal OB and converge to a single, posterior glomerulus (Fig. 7). In *Bbs8*-null animals, however, multiple glomeruli are innervated and axon fasciculation is impaired, with individual "wandering" fibers observed (Fig. 7). To determine whether these defects are present at birth, glomerular targeting was assessed in OB sections from *Bbs8* mice crossed to the *P2*^{TL} reporter line; the P2 glomerulus matures earlier than the M72 structure. Glomerular targeting-efficiency scores were assigned and revealed perturbed targeting in PD0 *Bbs8*$^{-/-}$ mice (Fig. S7). These observations suggest that aberrant cilia and the concomitant mislocalization of cilia-targeted transduction proteins at the dendritic end of the cell can have significant consequences for axon extension.

Discussion

We have generated a mouse model of BBS with robust reporter expression that reveals unique aspects of the olfactory phenotype associated with this disease and affords molecular insights into mechanisms by which perturbations in cilia may lead to defects in activity and alterations in olfactory axon targeting. *Bbs8*-null mice display phenotypes similar to other available mouse models of this disorder, including consistent genotype/phenotype correlations that contrast with the heterogeneity in BBS patients, perhaps reflecting heterogeneous genetic modifiers not reflected

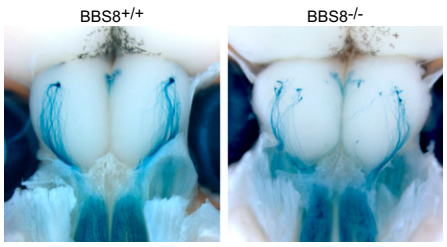

Fig. 7. OSN axon targeting is perturbed in *Bbs8*$^{-/-}$ mice. The OR reporter line M72^{TL} was crossed into a *Bbs8* mutant background and axon targeting was analyzed by whole-mount X-Gal staining of PD15 mice. In dorsal views, axons project from the OE (on the bottom) to their targets in the OB. In *Bbs8*$^{+/+}$ mice, M72-tau:lacZ–expressing axons converge to one dorsal glomerulus in each bulb. In the OB of *Bbs8*-deficient mice, multiple glomeruli are innervated and individual fibers wander on the surface of the bulb.

NEUROSCIENCE

in the mouse. The olfactory loss in adult *Bbs8*$^{-/-}$ mice closely parallels that observed in other BBS mutations (15), and decreased suckling associated with defects in this sensory system (27) likely accounts for the smaller early size and neonatal lethality.

Role of BBS8 in Cilia Dynamics. BBS8 is found within the OSN dendritic knob in a distribution distinct from γ-tubulin, a centriolar marker. This localization positions BBS8 at the base of cilia, where it could participate in a gate-keeping mechanism that allows only appropriate proteins access to the ciliary compartment. Consistent with this hypothesis, SLP3:eGFP protein is restricted and highly enriched in the most proximal portions of WT olfactory cilia but is dispersed throughout cilia in *Bbs8*-null OSNs. Similarly, BBS-like phenotypes arise from mislocalization of septins, which may function as a diffusion barrier at the base of cilia and as regulators of ciliogenesis (28, 29). An alternative explanation is that BBS8, as part of the BBSome, removes unwanted proteins from distal cilia, as been suggested in chlamydomonas (10). This model would require that BBS8 enter olfactory cilia, and although we did not see obvious immunostaining within cilia, we cannot exclude that steady-state levels within this compartment are below our detection levels.

Adult *Bbs8*-null mice display a dramatic reduction in olfactory cilia consistent with observations in *Bbs1*- and *Bbs4*-null mice (15). This cilia loss eliminates the platform for odorant detection and is likely to be the principal cause of the reduced EOG response. The retention of apparently normal cells and tissue architecture in the olfactory system affords an opportunity to examine the sequelae of cilia dysfunction in a stable sensory tissue and contrasts with degeneration in other sensory systems. For example, photoreceptors are lost via apoptosis, concomitant with inner and outer segment degeneration (3, 4, 12, 13). The capacity of OSNs to assess cilia status and either halt their initial growth or jettison faulty appendages might underlie these differences.

The ability of OSNs to constantly regenerate over the lifetime of an animal results in neurons of various ages and developmental stages coexisting within the mature epithelium. Although there are no effective methods for identifying cilia associated with young and old cells, the rare, long SLP3:eGFP-filled cilia observed in *Bbs8*-null mice may represent nascent OSNs that have not yet lost cilia and down-regulated levels of SLP3. This scenario would also explain the marked mosaicism in SLP3 expression observed in the *Bbs8*-null OE.

In addition to the structural loss of olfactory cilia, proteins destined for the dendritic knob and/or cilia mislocalize to the olfactory dendrite and cell body (Fig. 3 *B* and *C*). This phenotype could simply represent a cellular "traffic jam" because the ultimate destination of these proteins is compromised. In this scenario, the intracellular trafficking mechanisms responsible for moving newly synthesized proteins from the cell body to the apical regions of OSNs are still intact and functional. Alternatively, mislocalization could result from a primary defect in the trafficking machinery. We know little regarding how proteins move within this region of the OSN, and it is possible that BBS proteins play a role in trafficking within dendrites. Indeed, there is evidence that BBS proteins are involved more generally in intracellular transport (30–32).

Effect of *Bbs8* Disruption on OSN Activity and Axon Targeting. The retention of a normal epithelial organization and architecture allowed us to examine the consequences of structurally altered cilia while leaving the sensory cells intact. We hypothesized that cells that have chosen the same OR should have similar activity (and S100A5) levels, and this expectation was confirmed in WT mice. In contrast, S100A5 levels were highly variable in *Bbs8*$^{-/-}$ OE. The higher average S100A5 level in *Bbs8*-null OSNs compared with controls is inconsistent with the simple explanation that loss of cilia results in impaired signal transduction and lower levels of odorant activity-associated gene expression. Rather, it suggests that inappropriate transduction activity (either basal or odorant-induced) arising from second-messenger–generating machinery located in nonciliary compartments could elevate the transcriptionally regulated S100A5 levels. Indeed, signal for ORI7 and other transduction components is more intense in the dendrite and soma of *Bbs8*$^{-/-}$ OSNs vs. controls; this proximity to the nucleus likely exerts a greater effect on second-messenger–regulated transcription.

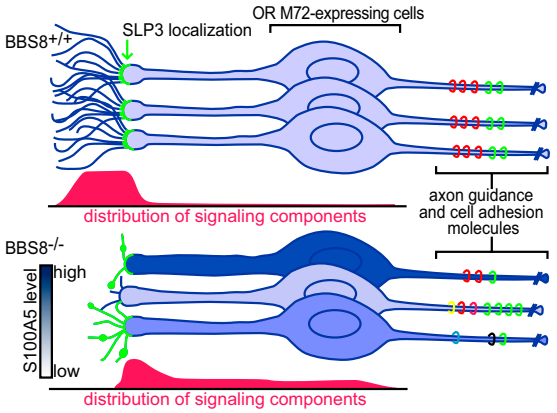

Fig. 8. Model for olfactory defects seen in *Bbs8*$^{-/-}$ mice. (*Upper*) In WT mice, the transduction proteins are restricted to a uniform complement of long cilia, resulting in consistent activity levels among cells expressing the same OR. Activity levels are correlated with abundance of axon guidance and cell adhesion molecules (colored rings). (*Lower*) *Bbs8*$^{-/-}$ OSNs display variability in cilia number and morphology. This leads to increased heterogeneity in neuronal activity and corresponding variability in S100A5 levels among OSNs expressing the same OR, depicted as differently shaded OSNs. The greater variation in abundance and diversity of axon guidance and cell adhesion molecules on the OSN axons would affect the fidelity of targeting.

The process by which OSNs, intermingled within the OE and each expressing one of 1,000 distinct ORs, sort and innervate precise regions of the OB is complex (33). Axons are first routed to their approximate target via odorant-independent events, and targeting is then refined in an activity-dependent manner. This refinement is thought to occur by regulating the identity and abundance of axon guidance and cell adhesion molecules, including Kirrel 2/3 and BIG2 (22, 23), via canonical OR-mediated signaling. Our data are consistent with the above model of olfactory axon targeting. We observe that, in *Bbs8*$^{-/-}$ mice, most axons head toward the region where the glomerulus is stereotypically located, but convergence to a single glomerulus is impaired, perhaps because altered levels of adhesion molecules caused by dysregulated activity prevent maturation of glomerular targeting or alter efficacy of synapse stabilization.

Fig. 8 provides a speculative model to explain our results. We propose that loss of BBS8 causes variable defects in OSN cilia and mislocalization of transduction components. This causes dysregulation of odor-independent and -dependent signaling, seen in our experiments as hypervariable S100A5 levels. This dysregulation is likely to affect the identity and level of cell adhesion and axon guidance molecules expressed on OSN axons, resulting in heterogeneity among axons from OSNs expressing the same OR and the observed defects in axon targeting. In this way, anosmia could stem from the primary effects of BBS8 loss (loss of cilia), the secondary effects (miswiring of olfactory pathways), or both. It will be intriguing to learn whether additional BBS phenotypes arise as a secondary consequence of primary defects.

Methods

Mice. Targeting constructs for *Bbs8* and *SLP3*^{eGFP} were assembled via standard cloning techniques using DNA from 129/Sv BACs (Research Genetics) and targeting cassettes as previously described (24, 27). The *Bbs8* locus construct maintained upstream regulatory elements, deleted the start codon and first two exons, and integrated the tau:YFP reporter at the BBS8 start

codon. For *SLP3* targeting, sequences in the final two exons were replaced with a *SLP3* cDNA fragment such that the translation stop codon was eliminated and the *SLP3* ORF was fused to eGFP. $M72^{TL}$ and $P2^{TL}$ mice were kindly provided by P. Mombaerts (Max Planck Institute of Biophysics, Frankfurt, Germany).

The *Bbs8* knock-out was generated and maintained on a 129/Sv background. *SLP3*, *M72*, and *P2* mice were maintained as mixed 129/C57Bl6 by outcrossing and interbreeding. Genetic crosses between the *Bbs8* mice and the various reporters were used to establish lines. Unless otherwise noted, mice were adults between 1 and 4 mo of age. Within each experiment, controls were littermates or age-matched when possible.

In Situ Hybridization and Immunofluorescence. Full-length *Bbs8* cDNA sense and antisense probes were hybridized to paraformaldehyde (PFA)-fixed OE cryosections using a standard protocol (34). BBS8 antibodies were generated to BSA-conjugated peptide (HVDTQHLIKQLKQHFAML) from the BBS8 C terminus and affinity-purified. Tissues for immunofluorescence were harvested from mice perfused with PFA or Bouin's fixative, and 20-μm cryosections were cut from OB or OE. Primary antibodies used were as follows: BBS8 (rabbit, 1:100), γ-tubulin (mouse, 1:200; Abcam), acetylated tubulin (mouse, 1:1,000; Sigma), ACIII (rabbit, 1:1,000; Santa Cruz Biotechnology), ORI7 [guinea pig, 1:2,500; Y. Yoshihara (RIKEN Brain Science Institute, Saitama, Japan)], SLP3 (rabbit, 1:50) (20), lacZ (chicken, 1:500; Abcam), S100A5 (rabbit, 1:200) (24). Some primary antibodies (ORI7, lacZ) required antigen retrieval (5′ 100C in 10 mM Na citrate, pH 6.0). DAPI (1:10,000) was used to counterstain nuclei. Goat or donkey secondary antibodies were conjugated to Alexa Fluor 488, 546, and 633 (Molecular Probes). Images were taken using a Zeiss 510 confocal microscope. For the S100A5 experiment, identical microscope settings were used to obtain single confocal images of lacZ-positive OSNs chosen with the genotype and S100A5 intensity blinded to the experimenter. The signal intensity in the two channels was then analyzed using the Zeiss software by outlining the cell body using the lacZ signal and then determining the average pixel intensity within that region for both lacZ and S100A5. S100A5 levels were then normalized to lacZ intensity to account for differences in antibody accessibility.

SEM. Mice were killed and half-heads were dissected to expose the olfactory turbinates. Tissue was fixed (2.5% glutaraldehyde, 4% PFA, 10 mM CaCl2 in 0.1 M Hepes) for 2 hr at room temperature. After coating with 1% tannic acid and 1% Os04, samples were dehydrated through an ethanol series, critical-point-dried, and then imaged on a S-4800 field emission scanning electron microscope.

Electro-olfactogram Recordings. EOGs were performed essentially as previously described (35). Briefly, mice were killed and the head was dissected to expose the olfactory turbinates. Humidified air was directed at the turbinates, and the odorant pulse (60 ms) was delivered from the vapor phase of an equilibrated tube of diluted odorant. Odorants (Aldrich) were dissolved in DMSO and diluted in water.

Whole-Mount SLP3:eGFP Imaging. Mice were killed and dissected to expose the olfactory turbinates. The tissue was glued to a dish, which was then filled with PBS. A 63× immersion objective (NA = 0.95) was used to confocal-image the cilia layer en face. For $Bbs8/SLP3^{eGFP}$ mice, a multi-PMT (photo-multiplier tube) spectral detector collected emissions across broad wavelengths (505–590 nm), and linear unmixing was used to separate the signals from the tau:YFP (*Bbs8*) reporter and the SLP3:eGFP fusion protein. Independent reference spectra for this separation were obtained from $Bbs8^{+/-}$ and $SLP3^{eGFP/eGFP}$ mice.

Whole-Mount X-Gal Staining. Mice were killed by an overdose of ketamine/xylazine and lightly perfused with 4% PFA. The dorsal aspect of the OBs and OE was exposed and stained overnight with X-Gal (1 mg/mL). Tissue was then rinsed in PBS and imaged using a Leica MZ FLIII stereomicroscope and Zeiss AxioCam CCD camera. Additional methods for supplemental information are described in *SI Methods*.

ACKNOWLEDGMENTS. We thank The Johns Hopkins University Transgenic Core for blastocyst injections, Y. Yoshihara for kindly providing the ORI7 antibody, and T. Watnick and D. Huso for examination of *Bbs8* kidneys.

1. Ansley SJ, et al. (2003) Basal body dysfunction is a likely cause of pleiotropic Bardet-Biedl syndrome. *Nature* 425:628–633.
2. Zaghloul NA, Katsanis N (2009) Mechanistic insights into Bardet-Biedl syndrome, a model ciliopathy. *J Clin Invest* 119:428–437.
3. Abd-El-Barr MM, et al. (2007) Impaired photoreceptor protein transport and synaptic transmission in a mouse model of Bardet-Biedl syndrome. *Vision Res* 47:3394–3407.
4. Davis RE, et al. (2007) A knockin mouse model of the Bardet-Biedl syndrome 1 M390R mutation has cilia defects, ventriculomegaly, retinopathy, and obesity. *Proc Natl Acad Sci USA* 104:19422–19427.
5. Mokrzan EM, Lewis JS, Mykytyn K (2007) Differences in renal tubule primary cilia length in a mouse model of Bardet-Biedl syndrome. *Nephron Exp Nephrol* 106: e88–e96.
6. Blacque OE, et al. (2004) Loss of C. elegans BBS-7 and BBS-8 protein function results in cilia defects and compromised intraflagellar transport. *Genes Dev* 18:1630–1642.
7. Ou G, Blacque OE, Snow JJ, Leroux MR, Scholey JM (2005) Functional coordination of intraflagellar transport motors. *Nature* 436:583–587.
8. Ou G, et al. (2007) Sensory ciliogenesis in Caenorhabditis elegans: Assignment of IFT components into distinct modules based on transport and phenotypic profiles. *Mol Biol Cell* 18:1554–1569.
9. Nachury MV, et al. (2007) A core complex of BBS proteins cooperates with the GTPase Rab8 to promote ciliary membrane biogenesis. *Cell* 129:1201–1213.
10. Lechtreck KF, et al. (2009) The Chlamydomonas reinhardtii BBSome is an IFT cargo required for export of specific signaling proteins from flagella. *J Cell Biol* 187: 1117–1132.
11. Jin H, et al. (2010) The conserved Bardet-Biedl syndrome proteins assemble a coat that traffics membrane proteins to cilia. *Cell* 141:1208–1219.
12. Mykytyn K, et al. (2004) Bardet-Biedl syndrome type 4 (BBS4)-null mice implicate Bbs4 in flagella formation but not global cilia assembly. *Proc Natl Acad Sci USA* 101: 8664–8669.
13. Nishimura DY, et al. (2004) Bbs2-null mice have neurosensory deficits, a defect in social dominance, and retinopathy associated with mislocalization of rhodopsin. *Proc Natl Acad Sci USA* 101:16588–16593.
14. Swiderski RE, et al. (2007) Gene expression analysis of photoreceptor cell loss in bbs4-knockout mice reveals an early stress gene response and photoreceptor cell damage. *Invest Ophthalmol Vis Sci* 48:3329–3340.
15. Kulaga HM, et al. (2004) Loss of BBS proteins causes anosmia in humans and defects in olfactory cilia structure and function in the mouse. *Nat Genet* 36:994–998.
16. Fath MA, et al. (2005) Mkks-null mice have a phenotype resembling Bardet-Biedl syndrome. *Hum Mol Genet* 14:1109–1118.
17. Ross AJ, et al. (2005) Disruption of Bardet-Biedl syndrome ciliary proteins perturbs planar cell polarity in vertebrates. *Nat Genet* 37:1135–1140.
18. Riazuddin SA, et al. (2010) A splice-site mutation in a retina-specific exon of BBS8 causes nonsyndromic retinitis pigmentosa. *Am J Hum Genet* 86:805–812.
19. Tan PL, et al. (2007) Loss of Bardet Biedl syndrome proteins causes defects in peripheral sensory innervation and function. *Proc Natl Acad Sci USA* 104:17524–17529.
20. Goldstein BJ, Kulaga HM, Reed RR (2003) Cloning and characterization of SLP3: A novel member of the stomatin family expressed by olfactory receptor neurons. *J Assoc Res Otolaryngol* 4:74–82.
21. Shah AS, et al. (2008) Loss of Bardet-Biedl syndrome proteins alters the morphology and function of motile cilia in airway epithelia. *Proc Natl Acad Sci USA* 105:3380–3385.
22. Kaneko-Goto T, Yoshihara S, Miyazaki H, Yoshihara Y (2008) BIG-2 mediates olfactory axon convergence to target glomeruli. *Neuron* 57:834–846.
23. Serizawa S, et al. (2006) A neuronal identity code for the odorant receptor-specific and activity-dependent axon sorting. *Cell* 127:1057–1069.
24. Bennett MK, Kulaga HM, Reed RR (2010) Odor-evoked gene regulation and visualization in olfactory receptor neurons. *Mol Cell Neurosci* 43:353–362.
25. Zheng C, Feinstein P, Bozza T, Rodriguez I, Mombaerts P (2000) Peripheral olfactory projections are differentially affected in mice deficient in a cyclic nucleotide-gated channel subunit. *Neuron* 26:81–91.
26. Zou DJ, et al. (2007) Absence of adenylyl cyclase 3 perturbs peripheral olfactory projections in mice. *J Neurosci* 27:6675–6683.
27. Zhao H, Reed RR (2001) X inactivation of the OCNC1 channel gene reveals a role for activity-dependent competition in the olfactory system. *Cell* 104:651–660.
28. Hu Q, et al. (2010) A septin diffusion barrier at the base of the primary cilium maintains ciliary membrane protein distribution. *Science* 329:436–439.
29. Kim SK, et al. (2010) Planar cell polarity acts through septins to control collective cell movement and ciliogenesis. *Science* 329:1337–1340.
30. Chiang AP, et al. (2006) Homozygosity mapping with SNP arrays identifies TRIM32, an E3 ubiquitin ligase, as a Bardet-Biedl syndrome gene (BBS11). *Proc Natl Acad Sci USA* 103:6287–6292.
31. Tayeh MK, et al. (2008) Genetic interaction between Bardet-Biedl syndrome genes and implications for limb patterning. *Hum Mol Genet* 17:1956–1967.
32. Yen HJ, et al. (2006) Bardet-Biedl syndrome genes are important in retrograde intracellular trafficking and Kupffer's vesicle cilia function. *Hum Mol Genet* 15: 667–677.
33. Sakano H (2010) Neural map formation in the mouse olfactory system. *Neuron* 67: 530–542.
34. Wang SS, Lewcock JW, Feinstein P, Mombaerts P, Reed RR (2004) Genetic disruptions of O/E2 and O/E3 genes reveal involvement in olfactory receptor neuron projection. *Development* 131:1377–1388.
35. Zhao H, et al. (1998) Functional expression of a mammalian odorant receptor. *Science* 279:237–242.